2009 American Control Conference
Hyatt Regency Riverfront, St. Louis, MO, USA
June 10-12, 2009

Design and Experimental Validation of a Nonlinear Tracking Control Law for an Electrostatic Micromirror

Carlos G. Agudelo, Muthukumaran Packirisamy, Guchuan Zhu, and Lahcen Saydy

Abstract— **This work aims at demonstrating potential benefits of applying nonlinear control techniques to electrostatic micromirrors in order to extend their stable operational range and enhance the system's performance. A nonlinear tracking control based on feedback linearization and trajectory planning has been developed. Aspects essential to the implementation of such a system, such as prevention of the device from its destruction on contact, modeling and sensing schemes allowing for the removal of on-chip sensors, influence of the dynamics of the driving circuit on the performance, and characterization of the device, have been thoroughly addressed and practical solutions have been proposed. The experimentation is performed on a set-up built with low cost, commercial off-the-shelf (COTS) instruments and components in an ordinary laboratory environment. The experimental results show that the developed control system can achieve a stable operation beyond the pull-in position for both set-point and scanning controls.**

I. Introduction

The electrostatic micromirror is one of the most popular microelectromechanical systems (MEMS), which is used in a variety of scientific, commercial, and defense applications, such as adaptive optics [15], optical network switching [4], projection systems [16], and resonant microsensors [1], among others. However, electrostatic actuation results in highly nonlinear dynamics, giving rise to a saddle-node bifurcation, called "pull-in," which limits the stable open-loop operation to a small portion of the whole physically available range [12]. Extending the stable operation range and enhancing the performance of electrostatic MEMS constitute the main motivation of the majority of the works in the application of closed-loop control in this area. The work reported in the literature has addressed the application of a variety of techniques, in particular nonlinear control methods, to the control of diverse electrostatic micro-actuators [9], [10], [21], [19], [13], [11], as well as experimental implementations of closed-loop control algorithms for micromirrors [4], [3], [18], [6].

The present work deals with the design of nonlinear tracking control of a one-degree of freedom (1DOF) scanning micromirror. It emphasizes particularly issues related to the experimental implementation. More specifically, in order to ensure safe and repeatable operations, the micromirror is designed in such a way as to prevent the destruction of the structure due to, e.g., short-circuit when the moveable and fixed electrodes come into contact (intentionally or accidently). To this end, stopping mechanisms are considered in the design of micromirror. We will see later that this structure will also allow avoiding a singularity in the dynamics of the device associated to short-circuit, making the system model more reliable.

Another important issue that affects both micro-actuator design of and control algorithm development is the choice of state variable in the dynamic model. In the literature, it is common to take the charge as a state variable for describing the dynamics of electrostatic MEMS (see, e.g., [12], [10], and [20]). However, the implementation of on-chip charge measurement requires additional structures (see, e.g., [2]), besides electrical interference between the actuation and the sensing during the operation. To circumvent this problem, the actuation voltage across the device is taken instead as a state variable in the dynamic model. Consequently, on-chip charge sensing is no longer required. As voltage measurement is instantaneous and trivial to implement, we can expect to achieve a simple but reliable implementation of control systems. A position sensitive detector (PSD) will be used as angular deflection sensor. This makes it possible to implement new control systems with existing devices that are not equipped with on-chip position and charge sensors.

The model used in controller design incorporates also the dynamics of the driving circuit, including output impedance of the high-voltage amplifier used in the experimental system. Note that the output capacitance of the high voltage amplifier is usually of several orders of magnitude greater than that of the device. Therefore, it has an important impact on the performance of the system and cannot be ignored in practice.

Finally, to obtain the angular velocity required for controller implementation, we use the discrete derivative in order to respect the capability offered by the embedded computation platform. Closed-loop stability and system performance will be assessed by numerical simulation and experimental test.

The rest of the paper is organized as follows. Section II presents the micromirror and its dynamic model. Section III is dedicated to the control synthesis. Section IV introduces the experimental setup and the characterization of the micromirror. The results of the simulation study and the experimental test are reported in Section V. Finally, Section VI contains some concluding remarks.

This work was supported in part by the Natural Science and Engineering Research Council of Canada (NSERC).

C. G. Agudelo, G. Zhu, and L. Saydy are with the Department of Electrical Engineering, École Polytechnique de Montréal, P.O. Box 6079, Station Centre-Ville, Montréal, QC, Canada H3C 3A7.

M. Packirisamy is with the Department of Mechanical and Industrial Engineering, Concordia University, 1455 de Maisonneuve Blvd. West, Montréal, QC, Canada H3G 1M8.

978-1-4244-4524-0/09/$25.00 ©2009 AACC

II. The Micromirror and its Dynamic Model

The optical microscope graph of the micromirror used in the present work is shown in Fig. 1(a). This device consists of a typical rectangular torsional micromirror [17]. Two metal layers of the same area are deposited, one on the substrate to form the bottom electrode, and the other on the surface of the micromirror for light reflection and hinges to form the top electrode. A main novelty is the inclusion of a stopping mechanism implemented by a comb extension. Without this structure, every operation beyond the pull-in position can become destructive if the top electrode crashes onto the bottom one, which might happen in such operations as full range characterization and control near the full gap position. Moreover, the comb structure allows minimizing the contact surface and the elasticity of the comb fingers will help restoring the moveable electrode back from the contact position. This structure allows also reducing the effect of fringing fields due to the stopping mechanism. Therefore, it will not introduce significant modeling error.

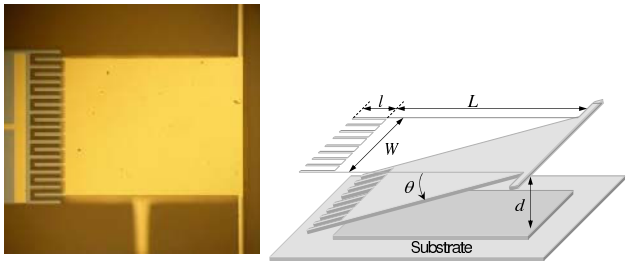

(a) (b)

Fig. 1. Micromirror: (a) Optical microscope graph of the fabricated device; (b) schematic representation of the structure.

The fabrication of the prototype is carried out by MicraGem process [17], which is well suited for uniform planar type devices. The air gap is 12μm and the thickness is 10μm. Other parameters of this device is given in Sections IV.

A schematic representation of the device is given in Fig. 1(b). The capacitance due to the electrostatic field between the two electrodes can be expressed as

$$C_a = C_0\gamma(\theta),$$

where C_0 is a constant representing the capacitance of the device at zero-voltage position. A dimensionless function of tilt angle $\gamma(\theta)$ is introduced to represent the variation of the capacitance. For the considered micromirror, the air gap is much smaller than the geometrical extent. Therefore the fringing field effect can be ignored. The capacitance of this device can then be computed as [20]

$$C_a = \varepsilon W \int_0^L \frac{dx}{d - x\sin\theta} = \frac{\varepsilon W}{\sin\theta}\ln\left(\frac{d}{d - L\sin\theta}\right), \quad (1)$$

where ε is the permittivity of air gap, W and L are, respectively, the width and the length of the electrodes, and d is the zero-voltage air gap. The capacitance at zero-voltage position is given by the well-known formula $C_0 = \varepsilon WL/d$ (see, e.g., [12]). Therefore the scaling function can be expressed as

$$\gamma(\theta) = \gamma_\theta = \frac{d}{L\sin\theta}\ln\left(\frac{d}{d - L\sin\theta}\right). \quad (2)$$

It can be verified by applying l'Hôpital's rule that $\gamma(0) = 1$, as expected. Note that $\gamma(\theta)$ has a singularity at contact position $\theta_C = \arcsin(d/L)$. With the stopping mechanism in the considered device, the actual contact will happen at position $\theta_{\max} = \arcsin(d/(L + l))$, where l is the comb extension length, which corresponds to the maximal tilt angle allowed by the geometry of the mirror. Since $\theta_{\max} < \theta_C$ if $l > 0$, the singularity in (2) will not occur.

The equation of motion of the micromirror is given by:

$$J\ddot{\theta} + b\dot{\theta} + k\theta = T_e, \quad (3)$$

where J is the mass moment of inertia of the moving electrode, b is the viscous damping coefficient, k is the stiffness coefficient, and T_e is the electrostatic torque. T_e can be computed by differentiating the stored electrical energy with respect to angular deflection [12]:

$$T_e = \frac{\partial}{\partial\theta}\left(\frac{1}{2}V_a^2C_a\right) = \frac{1}{2}V_a^2C_0\frac{\partial\gamma(\theta)}{\partial\theta} = \frac{1}{2}V_a^2C_0\gamma'_\theta \quad (4)$$

where V_a is the voltage across the device. It can be verified that γ'_θ is well defined for the structure considered except for the points of contact.

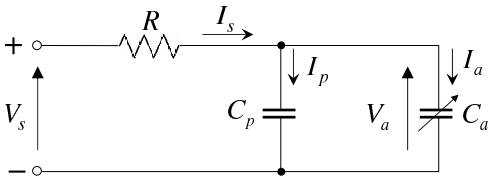

Fig. 2. Equivalent electrical circuit.

The dynamics of the electrical subsystem including output impedance of the high voltage amplifier can be deduced from the equivalent circuit of the system shown in Fig. 2 as

$$I_p + I_a = \dot{Q}_p + \dot{Q}_a = \frac{1}{R}(V_s - V_a), \quad (5)$$

where V_s is the source voltage, which is the actual control signal, and C_p is a constant capacitance including output capacitance of the voltage amplifier and parallel parasitics due to current leak. Then, the relationship

$$Q_a = C_aV_a, \quad Q_p = C_pV_a,$$

yields

$$\dot{Q}_a = C_a\dot{V}_a + \dot{C}_aV_a = C_a\dot{V}_a + C_0\gamma'_\theta\dot{\theta}V_a, \quad \dot{Q}_p = C_p\dot{V}_a.$$

It can be deduced from (5) that

$$\dot{V}_a = \frac{V_s - V_a}{RC_0\left(C_p/C_0 + \gamma(\theta)\right)} - \frac{\dot{\theta}\gamma'(\theta)V_a}{C_p/C_0 + \gamma(\theta)}. \quad (6)$$

Note that the output capacitance of the amplifier has the effect of slowing down the actuation transient, affecting

the dynamical behavior of the system. However, the static behavior of the system, in particular the pull-in position, remains unchanged.

Letting $\omega = \dot{\theta}$ be the angular velocity of deflection and defining $\rho = C_p/C_0$, then using (3), (4), and (6) the system model can be expressed in state-space form as:

$$\dot{\theta} = \omega \tag{7a}$$

$$\dot{\omega} = \frac{1}{J}\left(-b\omega - k\theta + \frac{C_0}{2}\gamma'_\theta V_a^2\right) \tag{7b}$$

$$\dot{V}_a = \frac{1}{\rho + \gamma_\theta}\left(\frac{V_s - V_a}{RC_0} - \omega\gamma'_\theta V_a\right) \tag{7c}$$

which is defined in the restricted state space $\mathcal{X} = \{(\theta, \omega, V_a) \subset \mathbb{R}^3 | \theta \in (-\theta_{\max}, \theta_{\max})\}$. Note that the micromirror will never reach $-\theta_{\max}$ even if the attractive force is released at $\theta_{\max}$, because the damping of the device is nonzero. Moreover, for simplicity, we do not take into account the contact dynamics at which the system exhibits a switching behavior [9].

III. Control Synthesis

The closed-loop controller design combines techniques of exact feedback linearization and trajectory planning [7], [5], [8]. The desired performance and operations can be specified through appropriate choices of reference trajectories, allowing control system tuning to be carried out in a systematic way.

A. Feedback Linearization

Here, the standard procedure of feedback control of flat systems is followed (see, e.g., [5]). First, take the tilt angle θ as the output of the system and compute its time derivatives until the input appears:

$$y = \theta \tag{8a}$$

$$\dot{y} = \dot{\theta} = \omega \tag{8b}$$

$$\ddot{y} = \dot{\omega} = \frac{1}{J}\left(-b\omega - k\theta + \frac{C_0}{2}\gamma'_\theta V_a^2\right) \tag{8c}$$

$$\dddot{y} = \ddot{\omega} = -\frac{b}{J}\dot{\omega} - \frac{k}{J}\dot{\theta} + \frac{C_0}{2J}\left(\gamma'_\theta 2V_a\dot{V}_a + V_a^2\gamma''_\theta\dot{\theta}\right), \tag{8d}$$

where $\gamma''_\theta = \partial^2\gamma(\theta)/\partial\theta^2$. Substituting $\dot{V}_a$ in (8d) by that given in (6), System (7) can then be put into the Brunovsky canonical form in the new coordinates $z_1 = \theta, z_2 = \dot{\theta}, z_3 = \ddot{\theta}$ via a diffeomorphic change of coordinates and a suitable feedback control. That is

$$\begin{aligned} \dot{z_1} &= z_2 \\ \dot{z_2} &= z_3 \\ \dot{z_3} &= v \\ y &= z_1 = \theta \end{aligned} \tag{9}$$

According to (7c) and (8d), the input v is of the form:

$$\begin{aligned} v = \dddot{\theta} = &\frac{C_0}{J}\gamma'_\theta V_a\left(\frac{1}{\rho + \gamma_\theta}\left(\frac{V_s - V_a}{RC_0} - \omega\gamma'_\theta V_a\right)\right) \\ &- \frac{b}{J}\dot{\omega} - \frac{k}{J}\dot{\theta} + \frac{C_0}{2J}V_a^2\gamma''_\theta\dot{\theta}. \end{aligned} \tag{10}$$

After some further computations, the linearizing feedback control V_s can be expressed as

$$\begin{aligned} V_s = &\frac{R}{\gamma'_\theta V_a}(\rho + \gamma_\theta)\left(Jv + b\ddot{\theta} + k\dot{\theta}\right) \\ &+ V_a\left(1 + RC_0\gamma'_\theta\dot{\theta} - \frac{RC_0\gamma''_\theta\dot{\theta}(\rho + \gamma_\theta)}{2\gamma'_\theta}\right). \end{aligned} \tag{11}$$

It can be seen that the control give in (11) is singular when $V_a = 0$. This is due to the fact that System (7) is not linearly controllable at this point, because the quadratic term of the electrical variable in (7b), V_a^2, prevents the control from influencing ω through the term linear in V_a. In the implementation an ad-hoc artifice for avoiding the singularity is used, which consists in applying a small bias voltage to keep the operational point away from the uncontrollable point. As the deflection is not very sensitive to the applied voltage near the zero-voltage position, this bias voltage will not significantly affect the operational range of the device.

B. Closed-Loop Tracking Control

Closed-loop tracking control can be tackled through the linearized system (9). Let $y_r(t)$ be the desired trajectory and denote by $e = y - y_r$ the tracking error. In order to track y_r, it suffices to choose v as

$$v = \dddot{y}_r - k_2(z_3 - \ddot{y}_r) - k_1(z_2 - \dot{y}_r) - k_0(z_1 - y_r). \tag{12}$$

Then the dynamics of the tracking error satisfy

$$\dddot{e} + k_2\ddot{e} + k_1\dot{e} + k_0 e = 0, \tag{13}$$

which is asymptotically stable at $e = 0$ provided $s^3 + k_2 s^2 + k_1 s + k_0$ is a Hurwitz polynomial. This can be achieved by appropriate choice of the gain of the tracking controller.

In practice, measurement of the angular velocity of the deflection is not available. Due to computational power limitation, simple angular velocity estimation is preferred over complex observer algorithms. The reconstruction of the angular velocity is then performed by the first order backward difference

$$\omega_k = \frac{\theta_k - \theta_{k-1}}{T_s}, \tag{14}$$

where T_s is the sample time. The closed-loop stability and the performance of this control scheme will be verified through numerical simulation and experimental test.

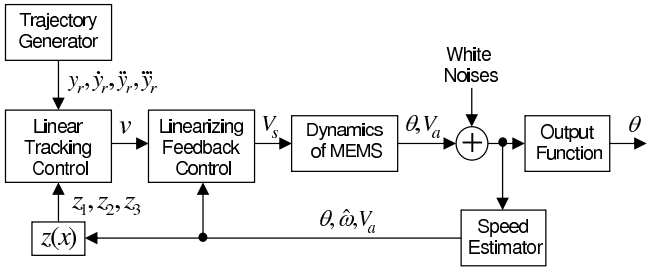

Fig. 3. Diagram of the closed-loop tracking control system.

Figure 3 shows the developed nonlinear tracking control scheme. The input and output signals of every block are indicated to illustrate the implementation procedure.

IV. Experimental Setup and Characterization of the Micromirror

A. Description of the Experimental Setup

A schematic representation of the experimental setup is shown in Fig. 4, which consists of an xPC Target-based control unit, a National Instruments 12bits DAQ (6025E), a high voltage (HV) amplifier (Apex PA97), an infrared laser source (900nm wavelength), and a PSD (S1880 of Hamamatsu). The electronic interfaces between the sensor, the actuator, and the DAQ board are custom-made circuits. During experimentation, the host controls and monitors the execution on the target. The main properties of the actuation system are listed in Table I. The value of the output resistance R is provided by the manufacturer and the output capacitance C_p is modeled by finding the *time constant* of a RC circuit that would deliver the same slew rate specified by the manufacturer. The acquisition of actuation voltage is implemented by a voltage divider.

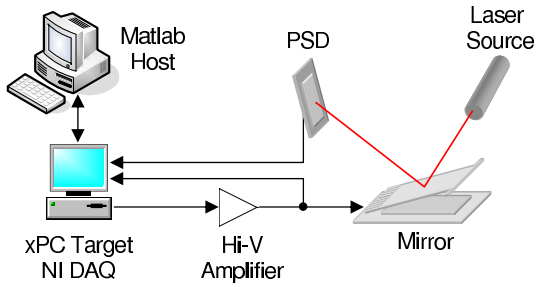

Fig. 4. Schematic representation of the experimental setup.

TABLE I
Parameters of the PA97 Amplifier.

Parameter	Value
Supply voltage	$\pm$300 (V)
Input impedance, DC	10^{11} (Ω)
Gain-bandwidth product	1 (Mhz)
Control voltage swing	$\pm$20 (V)
Output current	10 (mA)
Slew rate	8 (V/μs)
Output resistance R	100 (Ω)
Output capacitance C_p	2.0×10^{-7} (F)

B. Device Characterization

The characteristic of the micromirror is resumed in Table II. Geometrical parameters can be measured directly, while determining those related to the system dynamics, such as k, ω_n, ζ, θ_{PIN}, and V_{PIN} requires a more elaborated procedure. The aforementioned experimental setup is used for this purpose.

Figure 5 shows angular deflection of the micromirror to step inputs measured with a 100Mhz oscilloscope. Note that the rate of the applied voltage is limited by the slew rate of the HV amplifier.

The theoretical pull-in angle can be computed from ([14]):

$$\gamma'(\theta)|_{\theta=\theta_{PIN}} - \theta_{PIN}\gamma''(\theta)|_{\theta=\theta_{PIN}} = 0 \qquad (15)$$

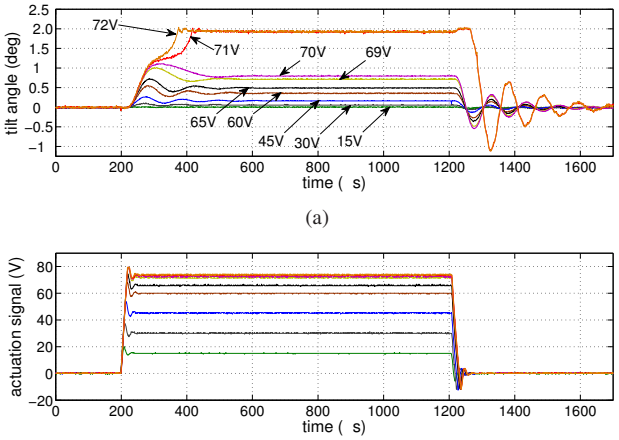

(a)

(b)

Fig. 5. Mirror response to step input: (a) tilt angles; (b) actuation signals.

TABLE II
Parameters of the Electrostatic Micromirror.

Parameter	Value
Mirror width W	250 (μm)
Mirror length L	300 (μm)
Mirror comb length l	50 (μm)
Air gap d	12 (μm)
Damping ratio ζ	0.06
Natural frequency ω_n	11 (KHz)
Stiffness coefficient k	2.1 10^{-7} (N/rad)
Contact angle θ_C	2.29°
Maximal angle $\theta_{\max}$	1.96°
Pull-in angle θ_{PIN}	1.0°
Pull in voltage V_{PIN}	70.6V
Permittivity ε	8.85×10^{-12} (F/m)

using the capacitance model (2), resulting in $\theta_{PIN} = 1.01°$. Note that this result agrees almost perfectly with the experimental pull-in angle shown in Table II. However, due to the dynamics of the electrical sub-system, open-loop control can only achieve a safe operation until $0.75°$.

In order to obtain the value of the stiffness coefficient k, the pull-in voltage V_{PIN} is determined based on laboratory tests. The value of k is computed by [14]

$$V_{PIN} = \sqrt{\frac{2k\theta_{PIN}}{C_0\gamma'(\theta)|_{\theta=\theta_{PIN}}}}. \qquad (16)$$

It is noted that the value of k must be particularly accurate since the pull-in voltage is very sensitive to this parameter.

From (3) it can be seen that around the equilibrium points the system behaves like a second order linear system. The damping ratio ζ and the undamped natural frequency ω_n can be determined in a straightforward manner from open-loop responses, using the well known relationships $J = k/\omega_n^2$ and $b = 2J\zeta\omega_n$.

V. Simulation Study and Experimental Validation

A. Simulation

The control law developed is firstly validated by means of numerical simulations with Matlab/Simulink. In order to

make the simulation as realistic as possible, the effect of quantization and measurement noise was taken into account with values similar to those used in practice. The angle resolution and the voltage resolution were set to 1.2mdeg and 0.2V, respectively. Uniformly distributed white noises varying between $\pm$10mdeg and $\pm$2V, respectively, were added to the outputs θ and V_a.

The generation of set-point control reference trajectories is based on the algorithm described in [8], which results in a polynomial of the following form:

$$y_r(t) = \theta(t_i) + (\theta(t_f) - \theta(t_i))\tau^5(t) \sum_{i=0}^{4} a_i \tau^i(t), \qquad (17)$$

where $\theta(t_i)$ is the initial tilt angle at time t_i, $\theta(t_f)$ is the desired tilt angle at time t_f, and $\tau(t) \triangleq (t - t_i)/(t_f - t_i)$. The coefficients in (17) can be determined by imposing the initial and final conditions

$$\dot{\theta}(t_i) = \dot{\theta}(t_f) = \ddot{\theta}(t_i) = \ddot{\theta}(t_f) = \theta^{(3)}(t_i) = \theta^{(3)}(t_f) = 0,$$

which yields $a_0 = 126$, $a_1 = -420$, $a_2 = 540$, $a_3 = -315$, and $a_4 = 70$.

Figure 6(a) shows the output θ for different set-points when a fixed-step solver cycling at 20μs is used. Note that this is the sampling rate used in experimental test. It can be seen that the developed controller makes the mirror angle follow the reference trajectory flawlessly up to a deflection of 1.4°. The simulation results also show that to further increase the amplitude of deflection, faster sampling rate is required. This is mainly due to the fast dynamics of the device. Figure 6(b) shows the corresponding control signals V_s. To avoid the singularity at zero-voltage position, a small bias voltage of $10V$ is applied, making the initial angle unnoticeably greater than zero (see beginning of the curves in Fig. 6(a)). Although quite smooth, it is seen that the control signal shows some variations near the uncontrollable point.

B. Experimental Test

The designed control system has been validated using the aforementioned experimental setup for both set-point control and scanning control. Every parameter has been set to the same as in numerical simulation. After some code optimizations the execution cycle has been brought down to 20μs, which is crucial for achieving a good performance for the system considered.

Figure 7(a) shows experimental results for different set-points below the pull-in position. The transition time for the reference was set to 20ms. It can be seen that the controller makes the micromirror follow the reference trajectory closely, hence delivering a satisfactory dynamic response. Figure 7(b) shows the control signals corresponding to different set-points. Similar to the simulation, the control signals show some vibrations near the uncontrollable point and are quite smooth elsewhere.

Figure 7(c) shows that stable operations beyond the pull-in position have been achieved with the developed closed-loop nonlinear control up to 1.4°, which represents 70.1% of

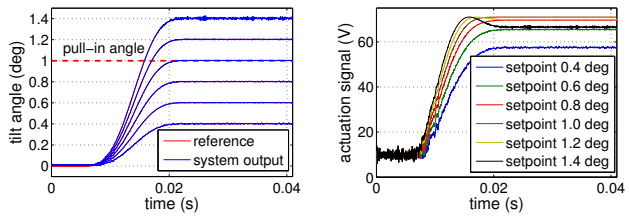

(a) (b)

Fig. 6. Closed-loop control simulation: (a) reference trajectories and system responses; (b) actuation signals.

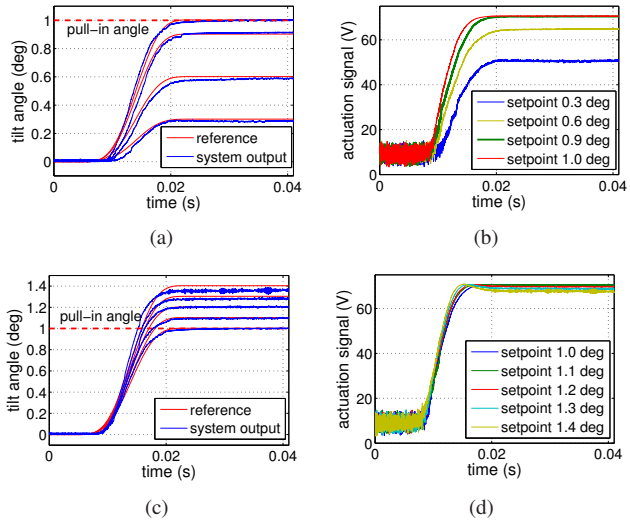

(a) (b)

(c) (d)

Fig. 7. Experimental test of the closed-loop set-point control: (a) system responses for set-points below the pull-in position; (b) actuation signals for set-points below the pull-in position; (c) system responses for set-points beyond the pull-in position; (d) actuation signals for set-points beyond the pull-in position.

the maximal deflection physically allowed by the structure or 87% of augmentation of the stable operational range compared to the open-loop control. It has been observed that for set-points beyond 1.5°, the system response becomes oscillating. This is mainly due to the limitation of sampling rate supported by our current setup. Therefore further improvements are still foreseen.

Despite the essentially satisfactory performance, there exists a small steady-state error for set-points corresponding to small and large deflections. The main reason for this is that the controller is tuned around the pull-in position. It is observed that the steady-state errors can be reduced by adequate parameter adjustment, in particular the stiffness coefficient which is assumed to be a constant in the model (3). Therefore, for further performance improvement, one should consider the use of more accurate models and control algorithms less sensitive to parameter variations. Another observation is the rather noisy system response for operations beyond the pull-in position as the open-loop system is not stable in this range. A great effort has been dedicated to decrease such noise as much as possible, but it is an unavoidable burden that real systems have to bear. Furthermore, stabilization beyond the pull-in position for the tested device

cannot be achieved for sampling rates slower than 28μs.

Figure 8 shows scanning operations that go beyond and below the pull-in position alternatively up to 1.3° with periods of 25ms, 50ms, and 100ms. Once again tracking controller exhibits a good performance managing the highly nonlinear control signals needed to achieve the prescribed trajectories. This confirms the versatility of the designed controller. Note that, however, as there is no guarantee that the control signal will be bounded away from 0, tracking of a faster reference trajectory might lead the system to a singularity.

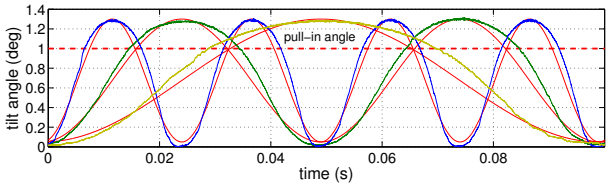

(a)

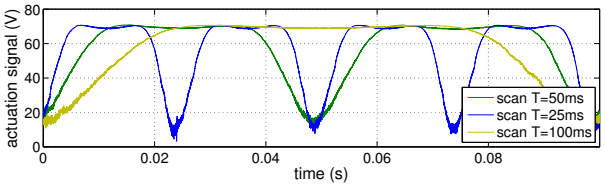

(b)

Fig. 8. Closed-loop scanning control beyond pull-in: (a) system responses, (b) actuation signals.

Finally, it is worth noting that all the presented results have been obtained using the same controller with the same tuning, which indicates a satisfactory robustness.

VI. Conclusions

This work addressed the control of a micromirror in order to obtain enhanced performance, in particular the capability of operating beyond the pull-in position. For this aim, a micromirror with short-circuit prevention mechanism has been designed and fabricated. A model with the actuation voltage as a state variable has been established which drastically simplified control system implementation. A nonlinear tracking controller has been developed, which can support diverse operations, such as set-point control and scanning control. Experimental tests show that the developed system can achieve a stable operation beyond the pull-in position and deliver a satisfactory performance. However, it is observed that to further improve the performance of the system, one needs to tackle modelling errors and parametric variations and to use more powerful real-time computational platform.

The experience of the present work confirms that considerations on control system design and implementation have an important impact on the design, the manufacturing process, the ease of integration, the reliability, and the cost of MEMS. Therefore this aspect must be taken into account at various stages of MEMS development.

References

[1] E. Abdel-Rahman, A. Nayfeh, and M. Younis, "Dynamics of an electrically actuated resonant microsensor," in *Proceedings. International Conference on MEMS, NANO and Smart Systems*, 2003, pp. 188–196.

[2] R. C. Anderson, B. Kawade, D. H. S. Maithripala, K. Ragulan, J. M. Berg, and R. O. Gale, "Integrated charge sensors for feedback control of electrostatic MEMS," in *Proc. of the SPIE conference on Smart Structures and Materials 2005*, San Diego, March 2005, pp. 42–53.

[3] J. Chen, W. Weingartner, A. Azarov, and R. C. Giles, "Tilt-angle stabilization of electrostatically actuated micromechanical mirrors beyond the pull-in point," *J. Microelectromech. Syst.*, vol. 13, no. 6, pp. 988–997, 2004.

[4] P. B. Chu and et al., "Design and nonlinear servo control of MEMS mirrors and their performance in a large port-count optical switch," *J. Microelectromech. Syst.*, vol. 14, no. 2, pp. 261–273, 2005.

[5] M. Fliess, J. Lévine, P. Martin, and P. Rouchon, "Flatness and defect of nonlinear systems: Introductory theory and examples," *Int. J. of Control*, vol. 61, pp. 1327–1361, 1995.

[6] S. Harshad, Y. Navid, and C. Mastrangelo, "Application of sliding mode control to electrostatically actuated two-axis gimbaled micromirrors," in *Proc. of the American Control Conference*, June 2003.

[7] A. Isidori, *Nonlinear Control Systems*, 3rd ed. London: Springer-Verlage, 1995.

[8] J. Lévine, *Analyse et Commande des Systèmes Non Linéaires*. [Online] http://cas.ensmp.fr/∽levine/Enseignement/CoursENPC.pdf, 2004.

[9] D. H. S. Maithripala, J. M. Berg, and W. P. Dayawansa, "Control of an electrostatic MEMS using static and dynamic output feedback," *ASME Journal of Dynamic Systems, Measurement and Control*, vol. 127, pp. 443–450, 2005.

[10] D. H. S. Maithripala, B. D. Kawade, J. M. Berg, and W. P. Dayawansa, "A general modelling and control framework for electrostatically actuated mechanical systems," *Int. J. Robust Nonlinear Control*, vol. 15, pp. 839–857, 2005.

[11] M. Malisoff, F. Mazenc, and M. de Queiroz, "Tracking and robustness analysis for controlled microelectromechanical relays," *Int. J. Robust Nonlinear Control*, 2007.

[12] S. D. Senturia, *Microsystem Design*. Norwell, MA: Kluwer Academic Publishers, 2002.

[13] K. P. Tee, S. S. Ge, and E. H. Tay, "Adaptive control of a class of uncertain electrostatic microactuators," in *Proc. of the 2007 American Control Conference*, New York City, USA, July 11-13 2007, pp. 3186–3191.

[14] H. Toshiyoshi and M. C. Wu, "Design of electrostatic actuators for MOEMS applications," in *Proc. Symp. on Design, Test, Integration and Packaging of MEMS/MOEMS*, 2002, pp. 200–207.

[15] R. K. Tyson, *Introduction to Adaptive Optics*. SPIE Publications, 2000.

[16] P. F. van Kessel, L. J. Hornbeck, R. E. Meier, and M. R. Douglass, "A MEMS-based projection display," in *Proc. of the IEEE Integrated Sensors, Microactuators, and Microsystems (MEMS)*, vol. 86, no. 8, August 1998, pp. 1687–1704.

[17] J. You, M. Packirisamy, and I. Stiharu, "Study of an electrostatically actuated torsional micromirror with compliant planar springs," *Microsystems Technology.*, vol. 14, no. 1, pp. 7–16, 2007.

[18] Y. Zhao, F. E. H. Tay, F. S. Chau, and G. Zhou, "Stabilization of dual-axis micromirrors beyond the pull-in point by integral sliding mode control," *J. Micromech. Microeng.*, vol. 16, no. 7, pp. 1242–1250, May 2006.

[19] G. Zhu, J. Lévine, and L. Praly, "Improving the performance of an electrostatically actuated MEMS by nonlinear control: Some advances and comparisons," in *Proc. of the 44th IEEE CDC and ECC 2005*, Seville, Spain, December 12-15, 2005, pp. 7534–7539.

[20] G. Zhu, M. Packirisamy, M. Hosseini, and Y.-A. Peter, "Modelling and control of an electrostatically actuated torsional micromirror," *Journal of Micromech. Microeng.*, vol. 16, no. 10, pp. 2044–2052, 2006.

[21] G. Zhu, J. Penet, and L. Saydy, "Modeling and control of electrostatically actuated MEMS in the presence of parasitics and parametric uncertainties," *ASME Journal of Dynamic Systems, Measurement and Control*, vol. 129, no. 6, pp. 786–794, 2007.